PEO/LAGP hybrid solid polymer electrolytes for ambient temperature lithium batteries by solvent-free, “one pot” preparation

PEO/LAGP hybrid solid polymer electrolytes for ambient temperature lithium batteries by solvent-free, "one pot" preparation

Giulia Piana[a], Federico Bella[a], Francesco Geobaldo[b], Giuseppina Meligrana[a], Claudio Gerbaldi[a,*]

[a] *Group for Applied Materials and Electrochemistry (GAME Lab), Department of Applied Science and Technology (DISAT), Politecnico di Torino, Corso Duca degli Abruzzi 24, 10129, Torino, Italy*

[b] *Group for Sustainable Processes For Agro-Food Industry (SPA), Department of Applied Science and Technology (DISAT), Politecnico di Torino, Corso Duca degli Abruzzi 24, 10129, Torino, Italy*

Corresponding Author (*): Claudio Gerbaldi, e-mail: claudio.gerbaldi@polito.it, phone: +39 011 090 4643

Abstract

Here, we report hybrid solid polymer electrolytes (HSPE) obtained by rapid, truly solvent-free, thus scalable preparation process. HSPE composition is very simple: a LiTFSI added poly(ethylene oxide) (PEO) polymer matrix encompassing NASICON-type $Li_{1.5}Al_{0.5}Ge_{1.5}(PO_4)_3$ (LAGP) super Li^+ ion conducting ceramic. Homogeneous, self-standing, mechanically robust solid electrolyte films are obtained by simply mixing in "one pot" and hot pressing the solid mixture of dry powders at moderate temperature. Noteworthy, unlike several other super ionic conductors used for composite electrolytes, LAGP is relatively stable in air atmosphere and can be processed in a dry-room, which is more favorable, cheap and scalable than Ar-filled dry glove box for industrial fabrication of safe lithium batteries. The proper, homogeneous mixing of LAGP powder, PEO and LiTFSI leads to HSPE with interesting electrochemical behaviour in lab-scale lithium cells, especially under high current regimes, and even at ambient temperature. HSPE-based cells outperform the PEO-LiTFSI-based counterpart, in terms of specific capacity output (about 70% of the theoretical values retained at very high 2C rate), limited fading and excellent Coulombic efficiency (>99.5 %) even at low rate. Interfacial stability issues remain to be solved, chiefly linked to the reactivity of LAGP in contact with lithium metal, but results here proposed represent a step further towards truly all-solid-state batteries conceived for high energy/power technologies, assuring safety and performance in a wide range of operating conditions.

Keywords: lithium polymer battery; composite polymer electrolyte; poly(ethylene oxide); superionic conducting ceramic; ambient temperature cycling

1. Introduction

Lithium-ion batteries (LIBs) are the most efficient and popular electrochemical storage devices in the market, powering daily the large majority of our smart, portable electronic devices [1-3]. However, their limitations in terms of energy density, safety, cost and primary resources still hinder the complete transition towards truly electrified, battery-powered systems [4-6]. Great efforts are now being made by the scientific community to improve electrodes' capacity, optimize their active surface and lower their costs, not only in LIBs, but also in advancing, alternative storage technologies, such as lithium metal, sodium-ion, lithium-air and lithium-sulfur cells [7-10]. Nonetheless, innovation in the field must pair mandatorily with the progressive evolution of suitable electrolytes, which determine energy/power density, operational stability, durability, and, chiefly, safety of the batteries [11,12].

Safer, cheap and, eventually, super-thin batteries shapeable in different geometries can be fabricated by the use of all-solid-state electrolytes (solid polymer electrolytes, SPE), instead of liquid ones [13], the latter being flammable and requiring the presence of a solid separator to avoid short-circuiting. A large part of industrially mature quasi-solid and solid electrolytes so far are based on cheap polymer matrices, such as poly(ethylene oxide) (PEO) and poly(vinylidene fluoride) (PVdF) [14-16], even if other macromolecular structures (with and without single-ion conducting features) have been proposed and are under intensive investigation by research groups worldwide, including polycarbonates, polymethacrylates, polyurethanes, etc. [17-20].

More recently, crystalline inorganic super-ionic conducting solid electrolytes have drawn much attention thanks to their intrinsic advantages in terms of electrochemical and thermal stability, together with very high ionic mobility at ambient temperature [21-23]. As a matter of fact, these materials provide ionic conductivities in the range of 10^{-4}–10^{-2} S cm^{-1} at 25 °C, much higher than that of common SPE (rarely exceeding 10^{-5} S cm^{-1}) and competing with non-aqueous liquid counterparts [24]. In addition, they are single-ion conductors with a lithium transference number usually close to 1, which is important for high power outputs. Materials under study in LIBs include: perovskite lithium lanthanum titanate $Li_{0.05-3x}La_{0.5+x}TiO_3$ (LLTO) [25], garnet-type $Li_7La_3Zr_2O_{12}$ (LLZO) [26–29] and NASICON-type oxides such as $Li_{1+x}Al_xM_{2-x}(PO_4)_3$ (where M = Ge, Ti or Zr) [30–33]. Amongst them, besides possessing high ionic conductivity at room temperature (about 7×10^{-4} S cm^{-1}), NASICON-type materials are stable under ambient atmosphere as well as in the presence of water and atmospheric moisture [34].

Germanium-based $Li_{1.5}Al_{0.5}Ge_{1.5}(PO_4)_3$ (LAGP) is a promising candidate as solid electrolyte; it can easily be scaled-up with the existing industrial processes at a competitive price, its synthesis does not require inert atmosphere as it is less prone to phase transitions, differently from sensitive garnet-type LLZO [35]. With respect to its titanium-based (LATP) counterpart [36], LAGP shows lower ionic conductivity, but is expected to be more chemically stable towards lithium metal; indeed, Ti-containing solid electrolytes are well-known to undergo to the Ti^{4+} to Ti^{3+} reduction upon contact with lithium, that leads to an electronic and ionic mixed conductive interface (MCI), often causing cell instability [37]. Conversely, Ge-containing materials, comprising the LAGP phase are often reported in the literature to be rather stable [38], even if the Ge^{4+} to Ge^{x+} has been described by Hartmann et al. [37] by using X-ray photoelectron spectroscopy, which means that their direct contact with Li metal should be carefully avoided [39]. Due to their intrinsic nature, NASICON-type materials are brittle and suffer from high grain boundary resistance and poor interfacial contact. All these issues can be overcome by developing organic-inorganic composite (hybrid) electrolytes that couple a solid mixture of polymeric and ceramic materials, where the softness and elasticity of the polymer matrix ensures an easy manufacturing and buffers volume changes occurring during cell operation, while maintaining the intimate contact between cell components [40]. The hybrid solution should also mitigate the instability in contact with the lithium metal electrode [39].

For these reasons, PEO/LAGP hybrid materials have drawn popularity in the last few years, and some studies have reported their simple fabrication and favourable electrochemical behaviour [24]. In a first attempt, PEO was used as an additive (5 wt% or less) to bind the solid electrolyte ceramic particles in a LAGP pellet, concurrently ameliorating its mechanical properties and integrity upon operation [41]. Dendrite-free cells were also fabricated by adding $P(EO)_yLiTFSI$ [42] or a glassy [43] layer as a buffer between sintered inorganic LAGP and lithium metal; enhanced electrochemical properties were demonstrated in lithium cells with improved efficiency. LAGP/PEO hybrid films with a LAGP content from 0 to 90 wt% were successfully prepared by Jung *et al.* [44,45] by solution casting of LAGP, PEO and $LiClO_4$; the most performing electrolyte in terms of capacity retention in a $LiFePO_4$/Li cell was loaded with 60 wt% of ceramic and showed ionic conductivity of 8×10^{-6} S cm^{-1} and stable interfacial resistance versus lithium metal. By adding the plastic crystal succinonitrile (SN), the authors improved both the ionic conductivity and the cycling behaviour of the electrolyte, due to a more stable and efficient SEI (Solid Electrolyte Interface) layer formed. With a similar method, Zhao *et al.* [46,47] investigated the effect of LAGP particles size and morphology in hybrid electrolytes and demonstrated that, at the same LAGP content, smaller particle size results in higher conductivity (6.76×10^{-4} S cm^{-1} at 60 °C with 20 wt% LAGP), thanks to the PEO amorphization. By incorporating a similar

composite electrolyte in the $LiFePO_4$ cathode slurry [36], the lithium cell showed stable operation with minimized interfacial resistance.

In this work, truly all-solid-state, hybrid polymer/ceramic electrolytes (hybrid solid polymer electrolyte, HSPE) were formulated combining various amounts of LAGP dry powder in a PEO/LiTFSI dry polymer mixture, by a rapid, simple, solvent-free preparation procedure setup to be readily scalable on a large-scale at an industrial level (e.g., by common extrusion). As stated before, LAGP powder is not sensitive to air/moisture, which renders it easily processable in a common dry room (not under the inert atmosphere of a dry glove box) to get HSPE, which are then dried for electrochemical testing. HSPE-based cells outperform the SPE (PEO-LiTFSI) based counterparts, in terms of specific capacity output, limited fading and excellent Coulombic efficiency even at low current regime. To the best of our knowledge, this work represents the first example of a solvent-free process, rapid and scalable, without sintering steps to PEO/LAGP based HSPEs, and opens up promising prospects in the development of all-solid-state energy storage devices.

2. Materials and methods

2.1 Preparation of the solid polymer electrolytes

Polyethylene oxide (PEO, average M_w: 150.000, dried under vacuum at 60 °C for 24 h before use) and lithium bis(trifluoromethanesulfonyl)imide (LiTFSI, battery grade, dried under vacuum at 120 °C for 24 h) were obtained from Sigma Aldrich and Solvionic, respectively. LAGP ceramic powder was purchased from Toshima (Japan), with three populations having 0.6, 1.5 and 28 µm particle size (according to the supplier).

The compositions under study consisted simply of PEO, LiTFSI and LAGP in different ratios, as given in **Table 1.**

Table 1. *Composition of the different solid electrolytes under study.*

Sample name	PEO (wt%)	LAGP (wt%)	LiTFSI (wt%)	y (EO:Li)	r (Li:EO) = 1/y
$P(EO)_{20}LITFSI$	76	0	24	20	0.050
$P(EO)_{15}LITFSI$	70	0	30	15	0.067
LA-20	56	20	24	15	0.067
LA-40	42	40	18	15	0.067
LA-60	28	60	12	15	0.067

Dry LiTFSI and LAGP powders were thoroughly mixed at ambient laboratory temperature, and then PEO was added to the mixture and ground in an agate mortar. The mixed powders were then heated at 80 °C and gently blended until a soft paste was obtained, which was then formed into a homogeneous, truly solid film by hot-pressing at 80 °C at 15 bar between two non-tacky sulfurized paper sheets, to allow an easy peeling at ambient temperature, separated by a spacer to have a proper control of the final thickness at about 200 µm. All preparations steps were carried out in a dry room with a relative humidity of less than 2% (20 °C, 10 m^2; Soimar, Italy). This procedure yielded white, homogeneous, self-standing and mechanically robust solid HSPE membranes, which were dried under vacuum at 50 °C for 24 h and stored in an Ar-filled dry glove box (Jacomex GP2 Concept, O_2 < 5 ppm, H_2O < 1 ppm) for further characterization.

For comparison purposes, HSPEs were compared with LAGP-free $P(EO)_yLiTFSI$ SPEs (where *y* corresponds to the EO:Li molar ratio), which were obtained by the same, rapid, solvent-free preparation procedure.

2.2 Characterization of the solid electrolytes, lab-scale cell assembly and testing

The thermal stability of the different solid electrolytes under study was evaluated by thermo-gravimetrical analysis (TGA) in the temperature range between 40 and 700 °C under N_2 flux at a heating rate of 10 °C min^{-1} on a TG 209 F1 Libra® instrument from Netzsch.

Differential scanning calorimetry (DSC) was carried out under N_2 atmosphere with a DSC 204 F1 Phoenix (Netzsch) instrument equipped with a low temperature probe. Specimens were placed in aluminum pans, cooled from ambient temperature down to -80 °C and, then, heated at 10 °C min^{-1} up to 90 °C. After the first heating cycle, the samples were cooled again to -80 °C (-10 °C min^{-1}) and re-heated with the same scan program. The second heating scan is shown in this work. The glass transition temperature (T_g) was taken at the onset of the curve (the half-height point of the heat flow variation).

Ionic conductivity was measured by impedance spectroscopy (EIS) analysis in symmetric ECC-Std electrochemical test cells by EL-CELL (Germany), assembled inside the dry glove box. Each electrolyte sample was placed between two stainless steel discs separated by a ring spacer to perfectly maintain sample diameter and thickness (internal diameter = 14 mm and thickness = 200 µm), thus confirming results reproducibility. EIS spectra were recorded on a Bio-Logic VMP3 multichannel potentiostat with an A.C. potential of 10 mV in the frequency range between 600 kHz and 1 Hz. Before measurements, cells were kept at 80 °C overnight and, then, the temperature was stabilized at 25 °C in an environmentally controlled simulation chamber

(BINDER MK-53, ΔT±1 °C) for a precise temperature control. The ionic conductivity was measured between 25 and 80 °C, after at least 2 h stabilization at each of the testing temperatures to allow cells reaching the thermal equilibrium. The electrolyte bulk resistance was taken at the lowest value of –Im(Z) of the Nyquist plot (see *Figure S1* in the Supplementary Material), representing the right side of the high-frequency half semi-circle due to the parallel combination of the bulk resistance and the geometric capacitance. The ionic conductivity (σ) was calculated based on the following equation (eq. 1):

$$\sigma = LA^{-1} R_b^{-1} \quad \text{Eq. 1}$$

where σ is the ionic conductivity (S cm^{-1}), R_b the bulk resistance, and L and A are the thickness and area of the studied sample, respectively.

Lithium transport number of the films was measured in symmetric Li/electrolyte/Li cells, assembled by sandwiching the electrolyte sample under study between two lithium metal electrode discs (diameter = 18 mm), again a ring spacer was used to have precise control over diameter and thickness of the electrolyte. Before measurements, the cells were stored under open circuit conditions in the climatic chamber at 80 °C for 24 h. Before starting the experiment, the cell resistance was monitored by EIS and the measurement started only when the interface was stabilized. A constant potential of 20 mV was applied for 5 h and the resulting current was measured. To have a precise measurement of the initial current, the instrument measured one point every 0.2 s for the first 10 s and, then, every 1 s for the remaining test time. EIS spectra were acquired immediately before and after the chronoamperometry (10 mV, frequency range from 600 kHz to 0.1 Hz).

Interfacial properties were assessed in Li/electrolyte/Li cells assembled with the same configuration described above, and lithium plating/stripping was carried out at 60 °C at a constant current density of ± 0.2 mA cm^{-2} for 1 h per cycle.

The electrochemical stability window was evaluated at 60 °C by cyclic voltammetry (CV), to assess the eventual interface passivation after several cycles; the limits towards both cathodic and anodic potential values were obtained separately by scanning the cell potential from the OCV (open circuit potential) down towards -0.3 *vs.* Li^+/Li and, then, upward to 2.5 V *vs.* Li^+/Li (cathodic stability window) and from the OCV towards 5.0 V *vs.* Li^+/Li and, then, downward to 2.5 V *vs.* Li^+/Li (anodic stability window). Cu metal foil and carbon black coated Al foil were used as the working electrodes for cathodic and anodic scans, respectively, with Li metal discs as both the counter and the reference electrodes.

All-solid-state lab-scale Li metal cells comprised the solid electrolyte under study sandwiched between a Li metal anode (200 µm, Chemetall, now Albemarle) and a $LiFePO_4$ (LFP) composite cathode, both of them cut into disks of 2.54 cm^2 area; the assembly was then placed in a ECC

Std test cell in the LFP/electrolyte/Li configuration. Galvanostatic charge and discharge cycling was carried out on an ARBIN BT2000 battery tester, at different current regimes (from C/10 to 2C) over the potential limits of 2.5 and 4 V *vs.* Li^+/Li. Composite LFP cathodes were prepared by standard doctor blading, on an Al current collector foil, of a slurry of LFP (Clariant-LP2), conductive carbon (Shawinigan Black AB50, Chevron Corp) and PVdF (M_w = 534000, Sigma Aldrich) in the 70:20:10 weight ratio and dissolved in N-methylpyrrolidone (NMP, Sigma Aldrich). After drying overnight, electrodes were cut into disks and vacuum dried at 120 °C for 24 h before assembly in the test cells inside the dry glove box.

3. Results and Discussion

Several studies in the literature report about the effect of salt concentration in PEO-LiTFSI mixtures ($P(EO)_yLiTFSI$, with *y* = EO:Li molar ratio ranging from 2 to 50) [48-52] and the PEO molecular weight (typically ranging from 1 to 100 kg mol^{-1}) [53], as the main factors influencing the ionic transport and mechanical properties of SPEs.

In our experiments, PEO molecular weight was kept constant at 150 kg mol^{-1}. Due to the plasticizing role of the salt in the polymer [49], we experienced that mechanical integrity deteriorated when increasing LiTFSI content, and samples were not self-standing at ambient temperature for *y* values lower than ≈15. As a consequence, LAGP-free samples, namely $P(EO)_{15}LiTFSI$ and $P(EO)_{20}LiTFSI$, were used as platforms in this work, and also used as reference polymer electrolytes for comparison purposes. For a similar reason, LAGP content was limited to 60%, so as to obtain the optimal compromise between ionic mobility, electrochemical and mechanical properties; indeed, a higher amount resulted in brittle and very tough HSPE precursor pastes, very difficult to get in the form of a homogeneous, self-standing film and which cannot retain their mechanical integrity upon testing.

HSPE and SPE (200 µm thick) under study were homogeneous, self-standing, as shown in **Figure 1**. The addition of LAGP increased the opacity and the overall density of the materials. Compared to the LAGP-free $P(EO)_{15}LiTFSI$ sample, LA series of HSPE were more robust and more easy to handle at ambient conditions, while keeping rather unchanged their mechanical integrity, elasticity and partial flexibility.

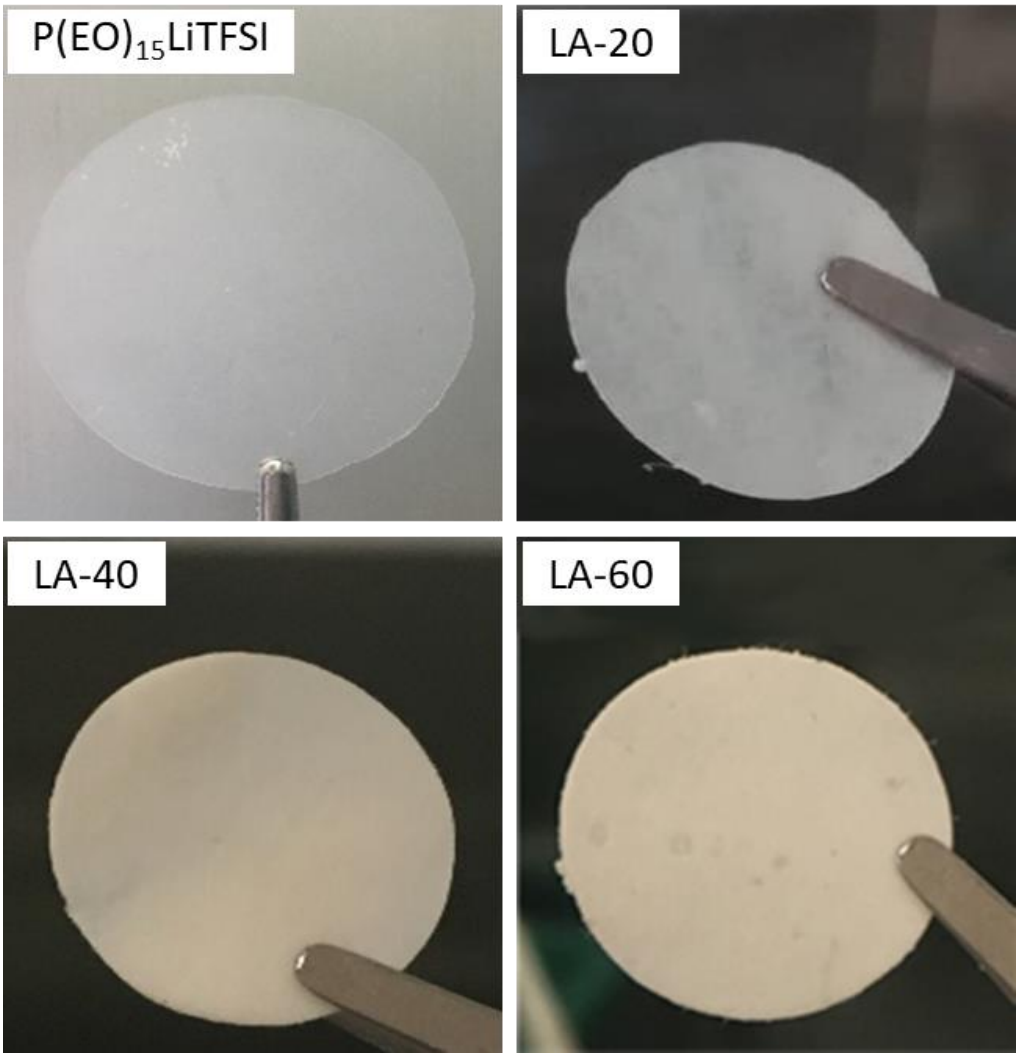

***Figure 1**. Digital photographs of the P(EO)$_{15}$LiTFSI solid polymer and the LA-20 to LA-60 series of hybrid solid polymer electrolytes under study (disk diameter: 18 mm).*

Thermal degradation behavior of the HSPE samples, measured by TGA experiments, is shown in **Figure 2a**. The faint weight loss below 100 °C is easily attributed to the removal of moisture that was absorbed during the preparation and loading of test samples. No further weight loss was observed until the irreversible decomposition starting at much higher temperatures. Thermal degradation, arbitrarily fixed when weight loss exceeded 10%, decreased with LAGP content increase in the samples. In LAGP-free P(EO)$_{15}$LiTFSI, degradation started at about 350 °C, while in LA-20, LA-40 and LA-60 degradation temperature was gradually reduced to 291, and 270-274 °C, respectively. This first weight loss is ascribed to the thermal degradation of PEO matrix and the decrease of the temperature underlined the modification of the crystalline phase occurring in the polymer when inorganic nanoparticles were introduced, as it will also be confirmed by DSC measurements shown in the followings. As compared to classic salt-in polymers, viz. PEO and lithium salt (LiX), the presence of ceramic particles, such as Al_2O_3 or ZrO_2, delays the

degradation process by a shielding phenomenon [54,55]. This extended degradation is generally attributed to the intercalation and exfoliation of the macromolecular chains in the presence of ceramic particles. Such interactions induce strong barrier effect preventing the polymer matrix from the thermal degradation [56]. However, in the present case, the interaction between the polymer chains that may lead to the exfoliation or intercalation may not occur, likely due to the large size of the ceramic particles. Moreover, the impurities that may be present at the surface of the ceramic particles (e.g., the precursors like lithium carbonate or ammonium dihydrogen phosphate) may catalyze the decomposition of the polymer chain in the presence of absorbed moisture from the polymer or from the environment. Above 400 °C, a second weight loss was detected, corresponding to LiTFSI salt degradation. The residual sample weight was found to be directly proportional to the ceramic phase introduced in the initial formulation, as a proof of the thermal and chemical stability of LAGP compound under the whole testing temperature.

DSC thermograms are shown in **Figure 2b**. Three distinct phase transitions can be observed, linearly correlated to the LAGP content in the samples. The glass transition temperature (T_g) was was determined to be −48.8 °C for the LAGP-free sample, in agreement with similar values found in the literature for materials having the same salt concentration [49]. In principle, LiTFSI is one of the best salts in terms of dissociation in PEO and also acts as a plasticizer, thanks to its ability to decrease the polymer crystalline phase. However, it is known that the ionic interactions between Li^+ and the oxygens are so strong that chains become less mobile inside the solid matrix and T_g increases with the salt content [57]. Similarly, the presence of LAGP in the HSPEs led to a less defined and higher T_g value that reached −39.9 °C in LA-60. This evolutions likely account for the formation of a continuous hybrid solid network with immobilized polymeric chains, even if this is just speculative due do the non perfect reliability of DSC analysis of composite polymer electrolytes. On the other hand, above 0 °C, the presence of LAGP particles hindered the recrystallization of the polymer network. However, a completely amorphous polymer electrolyte was not obtained by the preparation method adopted even after the addition of 15 and 60 wt. % of LiTFSI and LAGP, respectively. Only one melting peak (between 42 and 48 °C) is visible, demonstrating that only one organic phase was present in the samples, which accounts for no phase segregation in the samples, further highlighting the good salt dissociation promoted by PEO. As compared to classic composite polymers with PEO, LiX and Al_2O_3 or ZrO_2, the suppression of crystallization is less observed in the case of LAGP, which may be arising from the large particle size. Moreover, we observed that the inorganic powder slightly increased the melting temperature, being the latter also related to internal inter-/intra-chain physico-chemical interactions and corresponding decrease of the crystalline phase with increasing amount of LAGP.

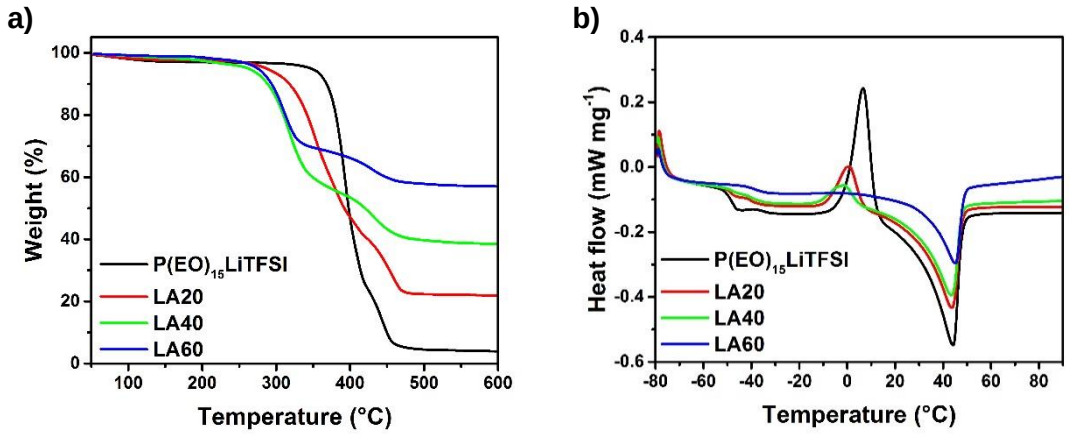

***Figure 2**. a) TGA thermograms under flowing N_2 (10 °C min^{-1}) and b) DSC traces under N_2 (10 °C min^{-1}) of the HSPE and SPE samples under study; DSC traces shown here are taken at the second heating cycle (see experimental).*

The evolution of the ionic conductivity in the temperature range between 25 and 80 °C is shown in **Figure 3a**. LAGP-free $P(EO)_{20}LiTFSI$ (EO:Li = 20:1) showed the typical profile of PEO-based electrolyte [58-60], with a phase transition at about 50-60 °C, where the crystalline phase melting occurs. At 25 °C, the ionic conductivity increased with LAGP content (see also **Figure 3b**), which is ascribed to the positive effect of the ceramic compound in the polymer electrolyte (note that a bare LAGP pellet shows a lithium ion conductivity around 2×10^{-4} S cm^{-1} at 25 °C [61]). In addition, contribution in terms of amorphization of the crystalline phase of the polymer by the ceramic particles may also contribute to the conductivity enhancement, as confirmed by the DSC results and the progressive disappearance of the previously described break in slope at around 50-60 °C when increasing the LAGP content in the samples. The sample with 60 wt. % of LAGP showed the best ionic conductivity value of 1.6×10^{-5} S cm^{-1} at low 20 °C temperature, *viz.* about one order of magnitude higher than that of the PEO-based SPE sample.

Considering that LA-60 has much higher mechanical robustness than bare PEO-LiTFSI based SPE, also encompassing a higher amount of lithium salt without losing its mechanical integrity, this is a remarkably high ionic conductivity value for a truly solid hybrid electrolyte at ambient temperature, even more appreciable if one considers the rapid, simple, ecofriendly and scalable preparation procedure if compared to conventional solution-casting all-solid-state electrolyte processing. The impedance responses, recorded on symmetrical two electrode cells, exhibit a faint half-semicircle at high frequencies, particularly at lower temperatures < 40 °C (see *Figure S1* in Supplementary Material) for the LA-40 sample (representative for all the samples prepared), suggesting phase separation likely due to hardening of the polymer matrix. At T≥40 °C, the impedance profiles are basically linear straight-lines, accounting for the homogeneous nature of the electrolyte mixtures. It is important to note that the ionic transport mechanism

likely varies depending on the composition (in particular, lithium path in hybrid ceramic/PEO species is still not fully understood, and work is in progress in our laboratories to shed light on this). Above 55 °C, PEO was in the melted state (as also shown by the DSC measurements) and pure $P(EO)_{15}LiTFSI$ electrolyte (LA-0) conductivity was higher than the HSPE counterparts. In this condition, chain motion is much more favorable without LAGP powder and ions find a much faster path through the full amorphous polymer matrix. However, at 80 °C we did not observe an obvious trend of the conductivity as a function of the LAGP quantity in the electrolyte. In these conditions, lithium transport may preferentially occur through PEO chains rather than through LAGP [51].

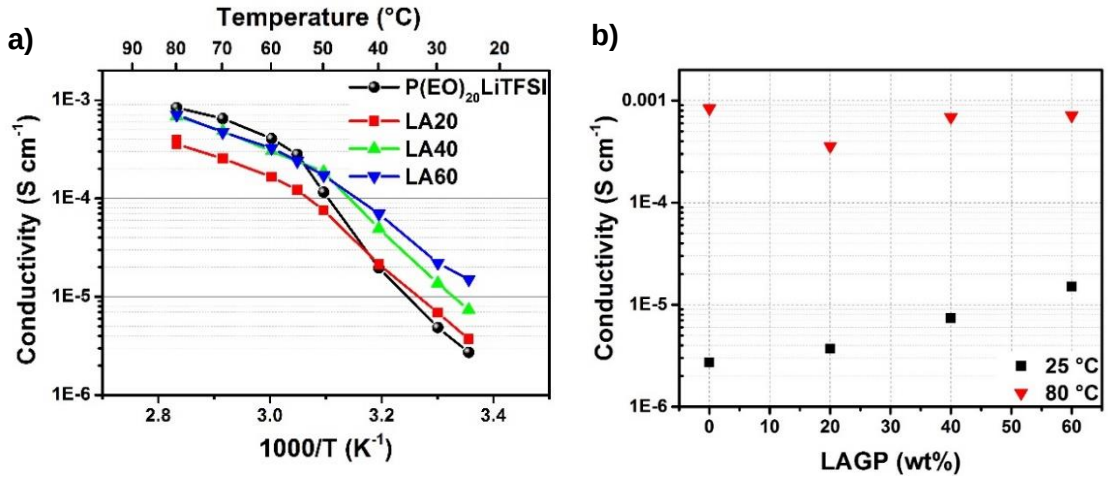

***Figure 3**. a) Temperature dependence of the ionic conductivity (Arrhenius plot) of the different SPE and HSPE electrolytes under study, and b) evolution of the ionic conductivity (measured at 25 and 80 °C) with the LAGP content in the different HSPEs.*

To provide more insights on the lithium transport mechanism in the HSPE under study, we made an attempt to calculate the lithium transport number by combined electrochemical analysis. The chronoamperometric measurement [62,63] consists in applying a constant potential in a Li/Li symmetric cell until all diffusive phenomena reach the steady state. Immediately before (time 0) and after (steady-state) the chronoamperometry, EIS analysis is performed to assess the interfacial resistances of the system. This technique considers a simplified electrolyte with completely dissociated lithium ions and is normally applied to $P(EO)_yLiTFSI$ electrolytes when EO:Li is higher than 30, or to very diluted electrolytic solutions. In the present case, lithium salt is more concentrated in the solid electrolyte and ionic or neutral complexes are likely to be formed and may affect the result [62]. However, at 80 °C we obtained rather reproducible results made on three different replicas for each of the HSPE compositions. Their evolution with LAGP content is plotted in *Figure S2* in Supplementary Material. To calculate lithium transport number

values, we used two different equations: the Bruce and Vincent (BV) equation (eq. 2) that measures the ratio between the initial current and the steady state current, corrected with the contribution of the electrolyte bulk resistance and the charge transfer resistance at the interfaces, and the equation (eq. 3) proposed by Watanabe *et al.* [64], which is comparable to *eq. 2* considering that there are not undesired side-reactions during the experiment. The advantage of *eq. 3* is that it is unnecessary to measure the value of I_0, which depends upon the parameters of both the measurement and the instrument (since it is correlated to the acquisition precision at time 0).

$$t_{+BV} = \frac{I_{ss}R_{b,ss}(\Delta V - I_0 R_{ct,0})}{I_0 R_{b,0}(\Delta V - I_{ss}R_{ct,ss})} \qquad \textit{(eq. 2)}$$

$$t_{+Wata} = \frac{I_{ss}R_{b,0}}{(\Delta V - I_{ss}R_{ct,ss})} \qquad \textit{(eq. 3)}$$

In both cases, ΔV is the applied DC potential (in V), I_0 and I_{ss} refer to the current flowing through the cell (in A) when the potential is applied at t_0 and when steady state is reached, respectively. R_b and R_{ct} are the values of the bulk and the charge transfer resistance of the cell, measured by EIS immediately before ($R_{b,0}$, $R_{ct,0}$) and after ($R_{b,ss}$, $R_{ct,ss}$) the potential is applied. If the system is at the equilibrium before the experiment starts (temperature and chemical interfaces), the resistance values are quasi-unchanged (especially R_b). Otherwise, the measurement must be repeated. LAGP is a single-ion conductor where the only conducting species is Li^+, and lithium transport number is therefore close to 1. In $P(EO)_yLiTFSI$ samples, transport number is usually reported to be in the range of 0.15 to 0.45, depending on the preparation process and the salt concentration [65]. In our experiments, LAGP-free samples showed a transport number equal to 0.21 (calculated by the BV method, slightly higher if calculated by the Watanabe equation), which is in accordance with the literature [15-17,49]. This transport number slightly increased with the LAGP content, although the effect was rather limited. This confirmed the previous hypothesis: at temperatures above PEO melting lithium transport chiefly occurs through the polymeric phase. Noteworthy, the LiTFSI content in LA-60 (12 wt. %) is more than three times lower than that of the LAGP-free SPE (39 wt. %), but transport number is not affected in the corresponding electrolytes, likely evidencing a role of LAGP in the ionic transport in the HSPE samples.

Figure 4 shows the electrochemical stability window of sample LA-60 evaluated in terms of cycling voltammetry (CV) in Li/LA-60/Cu cell towards cathodic potential values (cathodic stability window up to -0.3 V *vs.* Li^+/Li, Fig. 4a) and in Li/LA-60/Carbon black cell towards anodic potential values (anodic stability window up to 5.0 V *vs.* Li^+/Li, Fig. 4b) at 60 °C. Above 4.5 V *vs.* Li^+/Li, the oxidation of some of the electrolyte components took place. In our series of HSPE electrolytes,

PEO stability towards anodic potential is still the limiting factor, which was actually enhanced slightly by the addition of LAGP. Indeed, PEO-based polymer electrolytes are typically stable up to 4.1-4.2 V *vs.* Li^+/Li [15-17]. Noteworthy, the degradation observed for our system was very small (with a current density below 10^{-6} A cm^{-2} at 0.1 mV s^{-1}) and the interface seemed to be passivated after the first cycle up to 5.0 V *vs.* Li^+/Li, as confirmed by the absence of detectable reactions in the successive cycles. This latter, positive effect is important to guarantee a relative stability if high potential electrodes are used without any further passivating additives. The cathodic stability window is typical for a PEO – LiTFSI electrolyte and no straightforward effect due to the presence of LAGP could be observed in the experimental condition adopted. As provided in plot a) of Fig. 4, it shows well-defined and reproducible lithium plating/stripping processes, with very limited irreversible processes during the first cycle in the range 0.5–1.6 V vs Li^+/Li producing currents as low as ≈5 µA cm^{-2} attributed to the polymer matrix electrochemical activity that does not affect the overall behavior of the HSPE. The electrochemical stability was evaluated also at ambient temperature, confirming the rather high anodic potential window (see *Figure S3* in Supplementary Material).

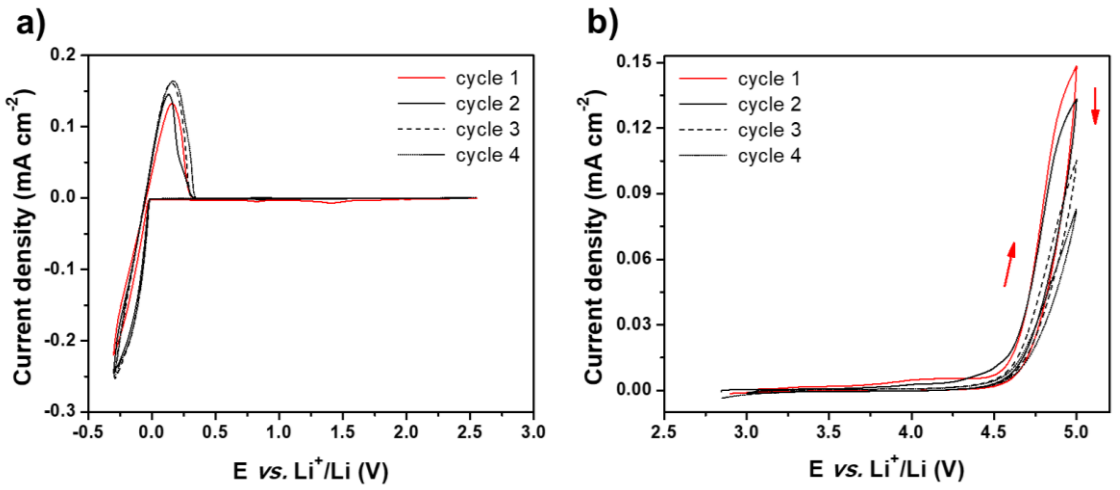

***Figure 4**. Electrochemical stability window of sample LA-60 obtained by cyclic voltammetry at 60 °C (potential scan rate of 0.1 mV s^{-1} for 4 cycles): a) cathodic stability plot, between -0.25 and 2.5 V vs. Li^+/Li (cell configuration: Li/LA60/Cu), and b) anodic stability plot between 2.5 and 5.0 V vs. Li^+/Li (cell configuration: Li/LA60/Carbon black).*

The compatibility (interfacial stability) of the electrolytes *vs.* lithium metal was evaluated in symmetric Li/electrolyte/Li cells by means of lithium plating and stripping experiments under a current density of 0.2 mA cm^{-2} for 1 h at 60 °C. The value and the stability of the recorded overpotential accounts for the electrolyte/lithium metal interfaces, and is indeed rather limited. It is known from the literature that NASICON-like electrolytes are reactive in contact with lithium

[37-39]. In fact, in-situ XPS measurements already showed that high valence state germanium in LAGP spontaneously reduced in contact with lithium metal ($Ge^{4+} \rightarrow Ge^{X+}$) and formed a mixed conducting interface (MCI) with both ionic and electronic conduction [37]. Generally, lithium protection is fundamental to allow stable operation with LAGP-based electrolytes.

In our present work, we used bare lithium metal electrodes, without any protective layers, and the resulting lithium plating and stripping experiments are shown in **Figure 5**, which compares the results of LA-60 (representative for the series of HSPE under study) and $P(EO)_{15}$LiTFSI SPE. In our experiments, a higher amount of LAGP (LA-40 and LA-60 samples) in the solid electrolytes resulted in substantial overpotential decrease during cycling, which likely accounts for continuous enhancement of the interfacial contact between the electron conductor (Li metal) and the ion conductor (PEO-LAGP framework). This is also evident in the plating/stripping test of LA-40 sample and the corresponding EIS spectra recorded every 10 plating and stripping cycles (20 h), shown in *Figure S4* in Supplementary Material, where the significant charge transfer resistance decrease is clearly evident, while the high frequency resistance (RHF) concurrently remains unchanged. After 40 h, RHF decreased from about 40 to 12 Ω, which could be an indication of MCI formation. The good cycling performance upon prolonged cycling is associated with an excellent Coulombic efficiency [66], which is fundamental to guarantee remarkable cycling performance in real cell configuration. After about 60 h of consecutive cycling, the overpotential of the Li metal electrode in the symmetric LA-60 based cell is smaller than that of the Li metal in the LAGP-free $P(EO)_{15}$LiTFSI based cell; it is likely ascribed to the improved ionic transport of the NASICON-type superionic conductor and the HSPE separating electrolyte film. Unfortunately, after 80-90 h, the cell failed gradually, as if it was degraded by multiple micro-short circuits, which means that the Li metal electrode in the solid-state HSPE-based cell is not free from dendritic lithium formation and/or surface reactivity issues. This result is consistent with what reported in the literature on NASICON-structured electrolytes, where cell failure was also observed after about 80 h in contact with non-treated lithium metal electrode [67]. Indeed, several studies confirmed the type of decomposition products, such as Li_2O, Li_2O_2, and Li_2CO_3 when Li metal is exposed to LAGP particles. According to Chung et. al. [68], the formation of lithium oxides at SEI layer can be accumulated, thus forming a thick layer. This Li_2O formation requires [O], which may be coming from the ceramic particles or even the polymer itself. This might lead to several complications at the surface resulting in a poor interface, cracks formation and/or limited dendrite resistance. Here, unfortunately, the presence of a prevalent PEO polymer phase was apparently not enough to passivate the lithium metal electrode, thus avoiding surface reactivity with LAGP. Various studies tackle this instability issue in the literature, introducing for example an inert buffer layer (conductive glass, polymer

electrolyte [69,70], ALD thin layer, artificial SEI [71], etc.) or a polymer-in-salt composite to avoid degradation, but this is not the purpose of this paper. In our present experiments, in order to effectively understand the interfacial stability upon prolonged cycling, we did not protected the lithium metal and, clearly, results still need to be properly optimized in terms of dendritic Li formation, but preliminary results are encouraging if one considers the solvent-free, cheap and scalable fabrication procedure of the HSPE.

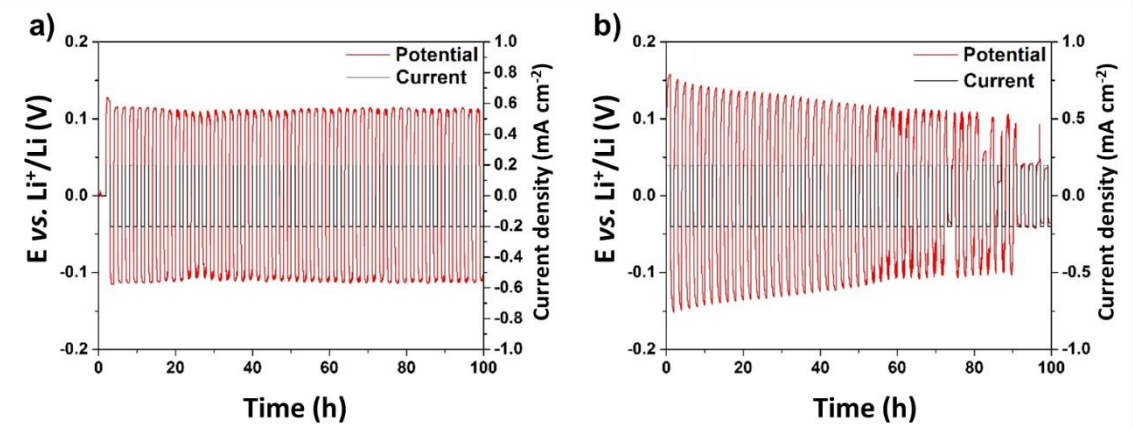

Figure 5*. Potential vs. time profiles during the Li plating and stripping experiments carried out in symmetric Li/electrolyte/Li cells assembled with: a) LAGP-free P(EO)$_{15}$LiTFSI, and b) LA-60 all-solid-state electrolytes under study (current density of ±0.2 mA cm^{-2} fixing each cycle to 1 h at 60 °C).*

In this respect, the following section demonstrates galvanostatic cycling successfully carried out for over 1200 h (approximately, 50 days) in an all-solid-state LFP-HSPE cell with a lithium metal anode.

First, constant current (galvanostatic) cycling was performed at 80 °C and different current rates (from C/10 to 2C), so as to understand the effect of LAGP in the polymer electrolytes. At this temperature, ionic conductivity of LAGP-free SPE and LA-60 HSPE are very similar; nonetheless, **Figure 6a** shows a clear enhancement of the specific capacity during cycling for the lithium cells assembled with the LAGP-based HSPE. Initial three cycles for each cell were carried out at low C/10 rate, corresponding to a current density of approximately 4×10^{-5} A cm^{-2} (given an active material mass for $LiFePO_4$ of ≈2.0 mg cm^{-2}). All of the HSPE-based cells demonstrated a very high initial specific capacity output in the range of 140 (LA-20) to 166 (LA-60) mAh g^{-1}, accounting for both the compatibility and suitability of the proposed hybrid electrolytes to operate with composite LFP cathodes and, more importantly, the good interpenetration/wetting of the electrolyte with the electrode. It is ascribed to the softening of the organic phase at 80 °C, which provides an optimal interfacial contact (even if the LFP cathodes are prepared without any ionic conductor) and leads to the efficient use of the active material particles through the whole

electrode thickness, which results in almost full capacity (LFP theoretical specific capacity = 170 mAh g^{-1}) for the LA-60 based cell. Noteworthy, the preparation of the hybrid ceramic/polymer solid-state electrolytes proposed in this work allows proper interfacial compatibility and operation with common porous electrodes having standard rough surface, unlike what is normally observed with truly solid bare ceramic LAGP in the form of pellets.

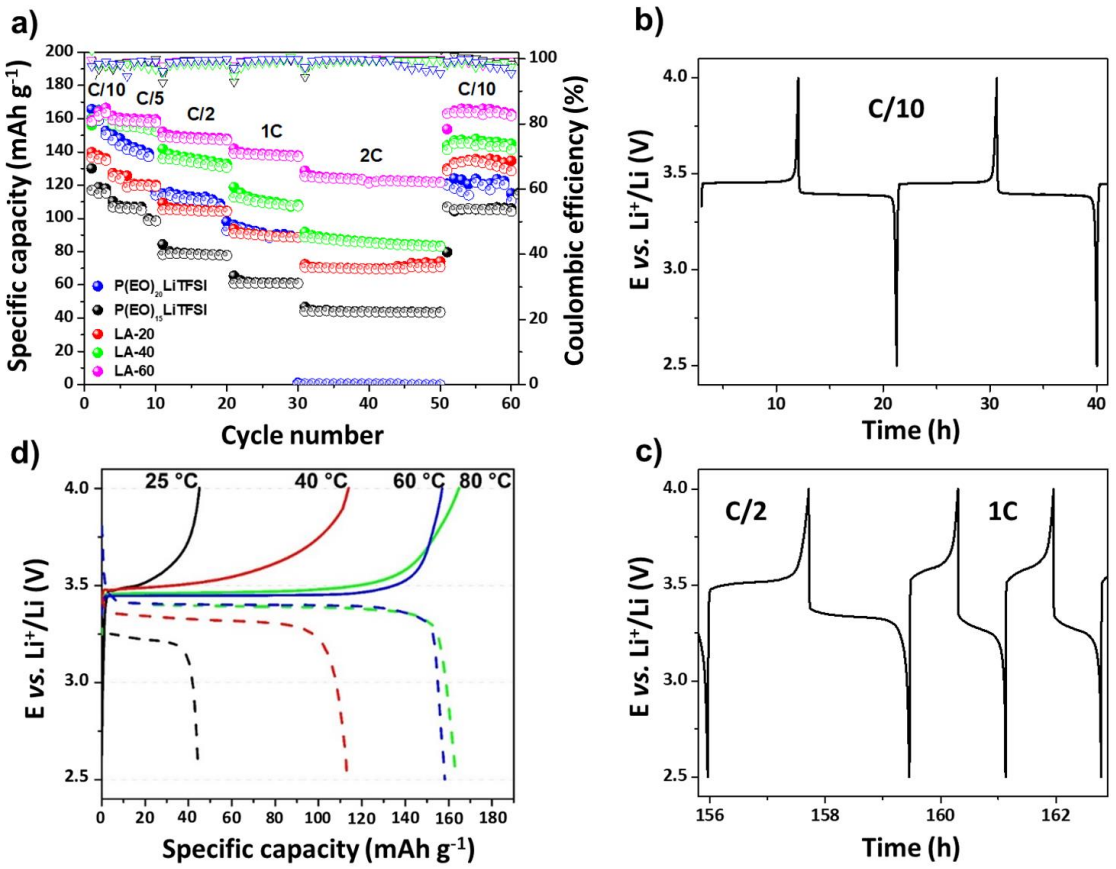

***Figure 6**. Electrochemical behaviour in terms of constant current (galvanostatic) cycling of the LFP/(HSPE or SPE)/Li cell under study: a) specific charge/discharge specific capacities at 80 °C and different current regimes (from C/10 to 2C), along with corresponding Coulombic efficiency values, b) potential vs. time profiles at C/10 rate of the LFP/LA-60/Li cell, c) potential vs. time profiles at C/2 and 1C rates of the LFP/LA-60/Li cell, d) potential vs. specific capacity profiles of the LFP/LA-60/Li cell at different temperatures (80 to 25 °C) and C/10 rate (charge and discharge profiles are shown as solid and dashed lines, respectively).*

The potential vs. time profiles extracted from galvanostatic cycling test of LFP/LA-60/Li cell, shown in **Figure 6b,c**, are neat and display a very flat conversion plateau, typical of LFP cathode, with small overpotential. Even at high 1C rate, the plateau is still clearly visible and flat, with limited overpotential for a truly solid Li metal cell. Interestingly, the rate capacity was effectively enhanced by the use of hybrid electrolyte encompassing LAGP. In particular, LA-60, laden with 60 wt% of LAGP powder, delivered the highest specific capacity in the excess of 125 mAh g^{-1} at

high 2C rate after 50 charge/discharge cycles, with excellent Coulombic efficiency exceeding 99.8 %. At the same current regime, LA-40 and LA-20 based cells provided 91 and 71 mAh g^{-1}, respectively. Conversely, LAGP-free cells based on bare PEO-LiTFSI demonstrated much lower specific capacity outputs, particularly at high current rates, which is another indication of the enhanced ion transport assured by LAGP. In addition, the comparison between two $P(EO)_yLiTFSI$ mixtures, with EO:Li = 15 and 20, highlights that a higher LiTFSI content in the SPE guarantees slightly better performances at higher current regimes, whereas a lower salt concentration causes a sudden drop to zero in the capacity above 1C regime. This effect was ascribed to the plasticizing effect of the salt and to the more efficient ion hopping between the polymer chains, as reported in the literature for super concentrated polymer electrolytes or polymer-in-salt systems [72]. After 50 cycles, all of the cells (except the one assembled with $P(EO)_{20}LiTFSI$ SPE) did not experience any abnormal drift upon cycling at high current densities, as confirmed by the full restoring of the capacity when the current was decreased back to C/10, thus accounting for the structural stability and mechanical integrity of the electrode/electrolyte materials upon cycling. The electrochemical behavior of HSPE-based cells is even more remarkable if one considers that the active material loading in the composite cathode is rather high for a truly solid cell, which accounts for a high current density flowing in the cell and through the electrolyte particularly at high 2C rate; in addition, one must consider that lab-scale Li metal cells in this work were assembled by standard sandwiching of electrodes and solid electrolyte and no electrolyte precursor was used to bind the active material particles, being out of the scope of the present work as it will limit the clear investigation of the HSPE properties.

Constant current charge/discharge cycling was carried out at different temperatures, from 80 °C down to ambient laboratory temperature, to test the capability of our HSPE under study to work in standard battery operational conditions. Li metal cells were assembled with the LA-60 electrolyte, which demonstrated the best performance at 80 °C. **Figure 6d** shows the potential vs. specific capacity profiles of the LFP/LA-60/Li cell at different temperatures and C/10 rate. The cell provided specific capacity values near the theoretical value at both 80 and 60 °C, in the excess of 100 mAh g^{-1} at 40 °C, and demonstrated proper operation with a clearly visible flat discharge plateau and about 45 mAh g^{-1} even at 25 °C, with an overpotential limited to about 0.25 V and high efficiency, which is remarkable for a truly solid hybrid polymer/ceramic electrolyte; once more, it accounts for the favorable electrochemical performance enhancement by the use of LAGP in the polymer matrix, which cannot be only ascribed to the plasticizing effect by the ceramic, but accounts for an improved - and not yet properly understood - transport mechanism in both organic and inorganic phases of the hybrid. On the contrary, as expected, SPE-based cells with standard $P(EO)_{15}LiTFSI$ electrolyte did not provide

any electrochemical response below 55 °C, *viz.* the PEO melting temperature because of the immobilized lithium ions in the crystalline phase. The above detailed results demonstrate that, by the use of hybrid polymer/ceramic electrolytes and the proper optimization of their composition, truly all-solid-state lithium metal cells can operate with stable performance and high efficiency in a wide temperature range, even down to ambient conditions; further intensive work as well as proper optimisation is needed, but here we have shown advancement towards fabrication of a practical and functional all-solid-state energy storage system at higher energy density and lower cost of production.

4. Conclusions

Efficient hybrid solid polymer electrolytes have been presented in this work, which were prepared by a rapid and, for the first time, truly solvent-free preparation process in "one pot". PEO-LiTFSI and LAGP were easily mixed and hot pressed at moderate temperature in a dry room, thus opening to an easily up scalable approach for Li-based battery solid-state electrolytes.

Hybrid electrolytes containing 60 wt.% of LAGP displayed the best ionic conductivity (1.6×10^{-5} S cm^{-1}) at low temperature, one order of magnitude higher than LAGP-free PEO-LiTFSI samples. The addition of LAGP enhanced the electrochemical stability window and transport characteristics of the materials. Truly interesting electrochemical performances in solid state lithium cells were obtained, especially under high current regimes (70% of the theoretical specific capacity at 2C and 80 °C), with limited fading and excellent Coulombic efficiency (>99.5 %) even at low rate. The LAGP-based cell was also cycled down to 25 °C at C/10 and still demonstrated stable cycling with the typical flat profile of $LiFePO_4$; conversely, LAGP-free electrolytes were not able to operate reversibly below the PEO melting temperature (i.e., 55 °C). Interfacial stability issues remain to be solved, chiefly linked to the reactivity of LAGP in contact with lithium metal, which we are trying to address now in our labs, but results here proposed represent a step further towards truly all-solid-state batteries conceived for high energy/power technologies, assuring safety and performance in a wide range of operating conditions.

Acknowledgements

The ENABLES project (http://www.enables-project.eu/) has received funding from the European Union's Horizon 2020 research and innovation programme, under Grant Agreement n° 730957. Ms. Marisa Falco is gratefully acknowledged for electrochemical stability window tests, plating/stripping and EIS of LA-40 sample, fruitful comments and discussions.

References

[1] G.-A. Nazri, G. Pistoia, Lithium Batteries: Science and Technology, 2009. doi:10.1007/978-0-387-92675-9.

[2] T.P. Narins, The battery business: Lithium availability and the growth of the global electric car industry, Extr. Ind. Soc. 4 (2017) 321–328. doi:10.1016/j.exis.2017.01.013.

[3] R. Wagner, N. Preschitschek, S. Passerini, J. Leker, M. Winter, Current research trends and prospects among the various materials and designs used in lithium-based batteries, J. Appl. Electrochem. 13 (2013) 481–496. https://doi.org/10.1007/s10800-013-0533-6

[4] S. Choi, G. Wang, Advanced Lithium-Ion Batteries for Practical Applications: Technology, Development, and Future Perspectives, Adv. Mater. Technol. 3 (2018) 1700376. doi:10.1002/admt.201700376.

[5] G. Martin, L. Rentsch, M. Höck, M. Bertau, Lithium market research – global supply, future demand and price development, Energy Storage Mater. 6 (2017) 171–179. doi:10.1016/j.ensm.2016.11.004.

[6] P. Meister, H. Jia, J. Li, R. Kloepsch, M. Winter, T. Placke, Best Practice: Performance and Cost Evaluation of Lithium Ion Battery Active Materials with Special Emphasis on Energy Efficiency. Chem. Mater. 28 (2016) 7203–7217. DOI: 10.1021/acs.chemmater.6b02895

[7] A. Kraytsberg, Y. Ein-Eli, A critical review-promises and barriers of conversion electrodes for Li-ion batteries, J. Solid State Electrochem. 21 (2017) 1907–1923. doi:10.1007/s10008-017-3580-9.

[8] G. Assat, J.-M. Tarascon, Fundamental understanding and practical challenges of anionic redox activity in Li-ion batteries, Nat. Energy. 3 (2018) 373–386. doi:10.1038/s41560-018-0097-0.

[9] T. Placke, R. Kloepsch, S. Dühnen, M. Winter, Lithium Ion, Lithium Metal, and Alternative Rechargeable Battery Technologies: the Odyssey for High Energy Density, J. Solid State Electrochem. 21 (2017) 1939–1964. https://doi.org/10.1007/s10008-017-3610-7

[10] L. Chen, L.–Z. Fan, Dendrite-free Li metal deposition in all-solid-state lithium sulfur batteries with polymer-in-salt polysiloxane electrolyte, Energy Storage Materials 15 (2018) 37-45. https://doi.org/10.1016/j.ensm.2018.03.015

[11] Q. Li, J. Chen, L. Fan, X. Kong, Y. Lu, Progress in electrolytes for rechargeable Li-based batteries and beyond, Green Energy Environ. 1 (2016) 18–42. doi:10.1016/j.gee.2016.04.006

[12] D. Larcher, J. M. Tarascon, Towards Greener and More Sustainable Batteries for Electrical Energy Storage, Nat. Chem. 7 (2015) 19–29. https://doi.org/10.1038/nchem.2085

[13] C. Sun, J. Liu, Y. Gong, D.P. Wilkinson, J. Zhang, Recent advances in all-solid-state rechargeable lithium batteries, Nano Energy. 33 (2017) 363–386. doi:10.1016/j.nanoen.2017.01.028.

[14] X. Cheng, J. Pan, Y. Zhao, M. Liao, H. Peng, Gel Polymer Electrolytes for Electrochemical Energy Storage, Adv. Energy Mater. 8 (2018) 1–16. doi:10.1002/aenm.201702184.

[15] L. Long, S. Wang, M. Xiao, Y. Meng, Polymer electrolyte for lithium polymer batteries, J. Mater. Chem. A 4 (2016) 10038-10069. DOI:10.1039/C6TA02621D

[16] E. Quartarone, P. Mustarelli, Electrolytes for solid-state lithium rechargeable batteries: recent advances and perspectives, Chem. Soc. Rev. 40 (2011) 2525–2540.

DOI:10.1039/C0CS00081G

[17] L. Yue, J. Ma, J. Zhang, J. Zhao, S. Dong, Z. Liu, G. Cui, L. Chen, All solid-state polymer electrolytes for high-performance lithium ion batteries, Energy Storage Mater. 5 (2016) 139–164. doi:10.1016/j.ensm.2016.07.003.

[18] Y. Tong, H. Lyu, Y. Xu, B. Prasad Thapaliya, P. Li, X.-G. Sun, S. Dai, All-solid-state interpenetrating network polymer electrolytes for long cycle life of lithium metal batteries, J. Mater. Chem. A 6 (2018) 14847-14855. DOI:10.1039/C8TA03062F

[19] H. Zhang, C. Li, M. Piszcz, E. Coya, T. Rojo, L.M. Rodriguez-Martinez, M. Armand, Z. Zhou, Single lithium-ion conducting solid polymer electrolytes : advances and perspectives, Chem. Soc. Rev. 46 (2017) 797-815. DOI:10.1039/C6CS00491A

[20] Y. Yu, F. Lu, N. Sun, A. Wu, W. Pan, L. Zheng, Single lithium-ion polymer electrolytes based on poly(ionic liquid)s for lithium-ion batteries, Soft Matter 14 (2018) 6313-6319. DOI:10.1039/C8SM00907D

[21] J.C. Bachman, S. Muy, A. Grimaud, H.H. Chang, N. Pour, S.F. Lux, O. Paschos, F. Maglia, S. Lupart, P. Lamp, L. Giordano, Y. Shao-Horn, Inorganic Solid-State Electrolytes for Lithium Batteries: Mechanisms and Properties Governing Ion Conduction, Chem. Rev. 116 (2016) 140–162. doi:10.1021/acs.chemrev.5b00563.

[22] C. Sun, J. Liu, Y. Gong, D. P. Wilkinson, J. Zhang, Recent Advances in All-Solid-State Rechargeable Lithium Batteries, Nano Energy 33 (2017) 363-386. https://doi.org/10.1016/j.nanoen.2017.01.028

[23] Z. Zhang, Y. Shao, B. Lotsch, Y. S. Hu, H. Li, J. Janek, L. F. Nazar, C. W. Nan, J. Maier, M. Armand, L. Chen, New Horizons for Inorganic Solid State Ion Conductors, Energy Environ. Sci. 11 (2018) 1945-1976. 10.1039/C8EE01053F

[24] P. Knauth, Inorganic solid Li ion conductors: An overview, Solid State Ionics. 180 (2009) 911–916. doi:10.1016/j.ssi.2009.03.022.

[25] Y. Inaguma, M. Nakashima, A rechargeable lithium–air battery using a lithium ion-conducting lanthanum lithium titanate ceramics as an electrolyte separator, J. Power Sources. 228 (2013) 250–255. doi:10.1016/J.JPOWSOUR.2012.11.098.

[26] K. Hayamizu, S. Seki, T. Haishi, Lithium ion micrometer diffusion in a garnet-type cubic $Li_7La_3Zr_2O_{12}$ (LLZO) studied using ^7Li NMR spectroscopy, J. Chem. Phys. 146 (2017) 024701. doi:10.1063/1.4973827.

[27] X. Yan, Z. Li, Z. Wen, W. Han, $Li/Li_7La_3Zr_2O_{12}/LiFePO_4$ all-solid-state battery with ultrathin nanoscale solid electrolyte, J. Phys. Chem. C. 121 (2017) 1431–1435. doi:10.1021/acs.jpcc.6b10268.

[28] S. Ramakumar, C. Deviannapoorani, L. Dhivya, L.S. Shankar, R. Murugan, Lithium garnets: Synthesis, structure, Li^+ conductivity, Li^+ dynamics and applications, Prog. Mater. Sci. 88 (2017) 325–411. doi:10.1016/J.PMATSCI.2017.04.007.

[29] Q. Liu, Z. Geng, C. Han, Y. Fu, S. Li, Y. bing He, F. Kang, B. Li, Challenges and perspectives of garnet solid electrolytes for all solid-state lithium batteries, J. Power Sources. 389 (2018) 120–134. doi:10.1016/j.jpowsour.2018.04.019.

[30] E. Zhao, F. Ma, Y. Guo, Y. Jin, Stable LATP/LAGP double-layer solid electrolyte prepared via a simple dry-pressing method for solid state lithium ion batteries, RSC Adv. 6 (2016) 92579–92585. doi:10.1039/C6RA19415J.

[31] F. Ma, E. Zhao, S. Zhu, W. Yan, D. Sun, Y. Jin, C. Nan, Preparation and evaluation of high

lithium ion conductivity $Li_{1.3}Al_{0.3}Ti_{1.7}(PO_4)_3$ solid electrolyte obtained using a new solution method, Solid State Ionics. 295 (2016) 7–12. doi:10.1016/J.SSI.2016.07.010.

[32] M. Monchak, T. Hupfer, A. Senyshyn, H. Boysen, D. Chernyshov, T. Hansen, K.G. Schell, E.C. Bucharsky, M.J. Hoffmann, H. Ehrenberg, Lithium Diffusion Pathway in $Li_{1.3}Al_{0.3}Ti_{1.7}(PO_4)_3$ (LATP) Superionic Conductor, Inorg. Chem. 55 (2016) 2941–2945. doi:10.1021/acs.inorgchem.5b02821.

[33] B. Commarieu, A. Paolella, J.-C. Daigle, K. Zaghib, Toward high lithium conduction in solid polymer and polymer–ceramic batteries, Current Opinion in Electrochemistry 9 (2018) 56-63. DOI: 10.1016/j.coelec.2018.03.033.

[34] Y. Cui, M.M. Mahmoud, M. Rohde, C. Ziebert, H. Juergen, Thermal and ionic conductivity studies of lithium aluminum germanium phosphate solid-state electrolyte, Solid State Ionics. 289 (2016) 125–132. doi:10.1016/j.ssi.2016.03.007.

[35] H. Chung, B. Kang, Increase in grain boundary ionic conductivity of $Li_{1.5}Al_{0.5}Ge_{1.5}(PO_4)_3$ by adding excess lithium, Solid State Ionics. 263 (2014) 125–130. doi:10.1016/J.SSI.2014.05.016.

[36] S. Cho, S. Kim, W. Kim, S. Kim, S. Ahn, S. Cho, S. Kim, W. Kim, S. Kim, S. Ahn, All-Solid-State Lithium Battery Working without an Additional Separator in a Polymeric Electrolyte, Polymers (Basel). 10 (2018) 1364. doi:10.3390/polym10121364.

[37] P. Hartmann, T. Leichtweiss, M.R. Busche, M. Schneider, M. Reich, J. Sann, P. Adelhelm, J. Janek, Degradation of NASICON-type materials in contact with lithium metal: Formation of mixed conducting interphases (MCI) on solid electrolytes, J. Phys. Chem. C. 117 (2013) 21064–21074. doi:10.1021/jp4051275.

[38] N. Kamaya, K. Homma, Y. Yamakawa, M. Hirayama, R. Kanno, M. Yonemura, T. Kamiyama, Y. Kato, S. Hama, K. Kawamoto, A. Mitsui, A Lithium Superionic Conductor, Nat. Mater. 10 (2011) 682–686. doi: 10.1038/nmat3066.

[39] D. Bosubabu, J. Sivaraj, R. Sampathkumar, K. Ramesha, LAGP|Li interface modification through a wetted polypropylene interlayer for solid state Li-ion and Li-S batteries, ACS Appl. Energy Mater. 2 (2019) 4118–4125. DOI: 10.1021/acsaem.9b00301.

[40] M. Keller, A. Varzi, S. Passerini, Hybrid electrolytes for lithium metal batteries, J. Power Sources. 392 (2018) 206–225. doi:10.1016/j.jpowsour.2018.04.099.

[41] Y. Li, F. Ding, Z. Xu, L. Sang, L. Ren, W. Ni, X. Liu, P. Spe, Ambient temperature solid-state Li-battery based on high-salt-concentrated solid polymeric electrolyte, J. Power Sources. 397 (2018) 95–101. doi:10.1016/j.jpowsour.2018.05.050.

[42] C. Wang, Y. Yang, X. Liu, H. Zhong, H. Xu, Z. Xu, H. Shao, F. Ding, Suppression of Lithium Dendrite Formation by Using LAGP-PEO (LiTFSI) Composite Solid Electrolyte and Lithium Metal Anode Modified by PEO (LiTFSI) in All-Solid-State Lithium Batteries, ACS Appl. Mater. Interfaces. 9 (2017) 13694–13702. doi:10.1021/acsami.7b00336.

[43] C. Wang, G. Bai, Y. Yang, X. Liu, H. Shao, Dendrite-free all-solid-state lithium batteries with lithium phosphorous oxynitride-modified lithium metal anode and composite solid electrolytes, Nano Res. 12 (2019) 217–223. doi:10.1007/s12274-018-2205-7.

[44] Y. Jung, S. Lee, J. Choi, S.S. Jang, D.-W. Kim, All Solid-State Lithium Batteries Assembled with Hybrid Solid Electrolytes, J. Electrochem. Soc. 162 (2015) A704–A710. doi:10.1149/2.0731504jes.

[45] Y.C. Jung, M.S. Park, C.H. Doh, D.W. Kim, Organic-inorganic hybrid solid electrolytes for

solid-state lithium cells operating at room temperature, Electrochim. Acta. 218 (2016) 271–277. doi:10.1016/j.electacta.2016.09.141.

[46] Y. Zhao, Z. Huang, S. Chen, B. Chen, J. Yang, Q. Zhang, F. Ding, Y. Chen, X. Xu, A promising PEO/LAGP hybrid electrolyte prepared by a simple method for all-solid-state lithium batteries, Solid State Ionics. 295 (2016) 65–71. doi:10.1016/j.ssi.2016.07.013.

[47] S. Chen, Y. Zhao, J. Yang, L. Yao, X. Xu, Hybrid solid electrolytes with excellent electrochemical properties and their applications in all-solid-state cells, Ionics 23 (2017) 2603–2611. doi:10.1007/s11581-016-1905-9.

[48] M.M. Hiller, M. Joost, H.J. Gores, S. Passerini, H.-D. Wiemhöfer, The influence of interface polarization on the determination of lithium transference numbers of salt in polyethylene oxide electrolytes, Electrochim. Acta 114 (2013) 21–29. doi:10.1016/j.electacta.2013.09.138.

[49] N.A. Stolwijk, C. Heddier, M. Reschke, M. Wiencierz, J. Bokeloh, G. Wilde, Salt-Concentration Dependence of the Glass Transition Temperature in PEO–NaI and PEO–LiTFSI Polymer Electrolytes, Macromolecules 46 (2013) 8580–8588. doi:10.1021/ma401686r.

[50] H.W. Kammer, Dielectric relaxation in PEO-based polymer electrolytes, Ionics (Kiel). (2017) 1–14. doi:10.1007/s11581-017-2290-8.

[51] D.M. Pesko, K. Timachova, R. Bhattacharya, M.C. Smith, I. Villaluenga, J. Newman, N.P. Balsara, Negative Transference Numbers in Poly(ethylene oxide)-Based Electrolytes, J. Electrochem. Soc. 164 (2017) E3569–E3575. doi:10.1149/2.0581711jes.

[52] N. Molinari, J.P. Mailoa, B. Kozinsky, Effect of Salt Concentration on Ion Clustering and Transport in Polymer Solid Electrolytes: A Molecular Dynamics Study of PEO-LiTFSI, Chem. Mater. 30 (2018) 6298–6306. doi:10.1021/acs.chemmater.8b01955.

[53] K. Timachova, H. Watanabe, N.P. Balsara, Effect of molecular weight and salt concentration on ion transport and the transference number in polymer electrolytes, Macromolecules. 48 (2015) 7882–7888. doi:10.1021/acs.macromol.5b01724.

[54] B. Liang, S. Tang, Q. Jiang, C. Chen, X. Chen, S. Li, X. Yan, Preparation and characterization of PEO-PMMA polymer composite electrolytes doped with nano-Al_2O_3, Electrochim. Acta 169 (2015) 334-341. https://doi.org/10.1016/j.electacta.2015.04.039.

[55] Y.H. Liao, X.P. Li, C.H. Fu, R. Xu, L. Zhou, C.L. Tan, S.J. Hu, W.S. Li, Polypropylene-supported and nano-Al_2O_3 doped poly(ethylene oxide)–poly(vinylidene fluoride-hexafluoropropylene)-based gel electrolyte for lithium ion batteries, J. Power Sources 196 (2011) 2115-2121. https://doi.org/10.1016/j.jpowsour.2010.10.062.

[56] N. Angulakshmi, K.S. Nahm, Jijeesh R. Nair, C. Gerbaldi, R. Bongiovanni, N. Penazzi, A. M. Stephan, Cycling profile of $MgAl_2O_4$-incorporated composite electrolytes composed of PEO and $LiPF_6$ for lithium polymer batteries, Electrochim. Acta 90 (2013) 179-185. https://doi.org/10.1016/j.electacta.2012.12.003.

[57] N. Angulakhsmi, S. Thomas, Jijeesh R. Nair, R. Bongiovanni, C. Gerbaldi, A. Manuel Stephan, Cycling profile of innovative nanochitin-incorporated poly (ethylene oxide) based electrolytes for lithium batteries, J. Power Sources 228 (2013) 294-299. http://dx.doi.org/10.1016/j.jpowsour.2012.11.007.

[58] F.M. Gray, J.A. Connor, Polymer Electrolytes, Royal Society of Chemistry, United Kingdom, 1997.

[59] M. Marzantowicz, F. Krok, J.R. Dygas, Z. Florjańczyk, E. Zygadło-Monikowska, The influence of phase segregation on properties of semicrystalline PEO:LiTFSI electrolytes, Solid State Ionics. 179 (2008) 1670–1678. doi:10.1016/j.ssi.2007.11.035.

[60] P. Lightfoot, M.A. Mehta, P.G. Bruce, Crystal Structure of the Polymer Electrolyte Poly (ethylene oxide)$_3$:LiCF_3SO_4, Science 262 (1993) 883–885. DOI: 10.1126/science.262.5135.883.

[61] C.R. Mariappan, C. Yada, F. Rosciano, B. Roling, Correlation between micro-structural properties and ionic conductivity of $Li_{1.5}Al_{0.5}Ge_{1.5}(PO_4)_3$ ceramics, J. Power Sources. 196 (2011) 6456–6464. doi:10.1016/j.jpowsour.2011.03.065.

[62] J. Evans, C.A. Vincent, P.G. Bruce, Electrochemical measurement of transference numbers in polymer electrolytes, Polymer 28 (1987) 2324–2328. doi:10.1016/0032-3861(87)90394-6.

[63] P.G. Bruce, J. Evans, C.A. Vincent, A dc technique for measurement of solid electrolyte conductivity, Solid State Ionics. 25 (1987) 255–262. doi:10.1016/0167-2738(87)90189-5.

[64] M. Watanabe, S. Nagano, K. Sanui, N. Ogata, Estimation of Li+ transport number in polymer electrolytes by the combination of complex impedance and potentiostatic polarization measurements, Solid State Ionics. 28–30 (1988) 911–917. doi:10.1016/0167-2738(88)90303-7.

[65] K. Pożyczka, M. Marzantowicz, J.R. Dygas, F. Krok, Ionic conductivity and lithium transference number of Poly(Ethylene Oxide):LiTFSI system, Electrochim. Acta. 227 (2017) 127–135. doi:10.1016/j.electacta.2016.12.172.

[66] C. Yang, L. Zhang, B. Liu, S. Xu, T. Hamann, D. McOwen, J. Dai, W. Luo, Y. Gong, E.D. Wachsman, L. Hu, Continuous plating/stripping behavior of solid-state lithium metal anode in a 3D ion-conductive framework, PNAS 115 (2018) 3770–3775. www.pnas.org/cgi/doi/10.1073/pnas.1719758115

[67] G. Hou, X. Ma, Q. Sun, Q. Ai, X. Xu, L. Chen, D. Li, J. Chen, H. Zhong, Y. Li, Z. Xu, P. Si, J. Feng, L. Zhang, F. Ding, L. Ci, Lithium Dendrite Suppression and Enhanced Interfacial Compatibility Enabled by an Ex Situ SEI on Li Anode for LAGP-Based All-Solid-State Batteries, ACS Appl. Mater. Interfaces. 10 (2018) 18610–18618. doi:10.1021/acsami.8b01003.

[68] H. Chung, B. Kang, Mechanical and Thermal Failure Induced by Contact between a $Li_{1.5}Al_{0.5}Ge_{1.5}(PO_4)_3$ Solid Electrolyte and Li Metal in an All Solid-State Li Cell, Chem. Mater. 29 (2017) 8611–8619. DOI: 10.1021/acs.chemmater.7b02301

[69] W. Zhou, S. Wang, Y. Li, S. Xin, A. Manthiram, J.B. Goodenough, Plating a Dendrite-Free Lithium Anode with a Polymer/Ceramic/Polymer Sandwich Electrolyte, J. Am. Chem. Soc. 138 (2016) 9385–9388. doi:10.1021/jacs.6b05341.

[70] Q. Li, J. Chen, L. Fan, X. Kong, Y. Lu, Progress in electrolytes for rechargeable Li-based batteries and beyond, Green Energy Environ. 1 (2016) 18–42. doi:10.1016/j.gee.2016.04.006.

[71] G. Hou, X. Ma, Q. Sun, Q. Ai, X. Xu, L. Chen, D. Li, J. Chen, H. Zhong, Y. Li, Z. Xu, P. Si, J. Feng, L. Zhang, F. Ding, L. Ci, Lithium Dendrite Suppression and Enhanced Interfacial Compatibility Enabled by an Ex-situ SEI on Li Anode for LAGP-based All-Solid-State Batteries, ACS Appl. Mater. Interfaces. 10 (2018) 18610–18618. doi:10.1021/acsami.8b01003.

[72] Z. Fang, Q. Ma, P. Liu, J. Ma, Y.-S. Hu, Z. Zhou, H. Li, X. Huang, L. Chen, Novel Concentrated

Li[(FSO_2)(n-$C_4F_9SO_2$)N]-Based Ether Electrolyte for Superior Stability of Metallic Lithium Anode, ACS Appl. Mater. Interf. 9 (2017) 4282–4289. doi:10.1021/acsami.6b03857.